BIOCHEMISTRY
including biophysical chemistry & molecular biology

ARTICLE

pubs.acs.org/biochemistry

Analysis of *Streptomyces coelicolor* Phosphopantetheinyl Transferase, AcpS, Reveals the Basis for Relaxed Substrate Specificity

Patrick Dall'Aglio,[†,] Christopher J. Arthur,[‡,] Christopher Williams,[‡] Konstantinos Vasilakis,[‡] Hannah J. Maple,[‡] John Crosby,[*,‡] Matthew P. Crump,[*,‡] and Andrea T. Hadfield[*,†]

[†]Department of Biochemistry, School of Medical Sciences, University of Bristol, University Walk, Clifton, Bristol BS8 1TD, U.K.

[‡]School of Chemistry, University of Bristol, Cantock's Close, Clifton, Bristol BS8 1TS, U.K.

Supporting Information

ABSTRACT: The transfer of the phosphopantetheine chain from coenzyme A (CoA) to the acyl carrier protein (ACP), a key protein in both fatty acid and polyketide synthesis, is catalyzed by ACP synthase (AcpS). *Streptomyces coelicolor* AcpS is a doubly promiscuous enzyme capable of activation of ACPs from both fatty acid and polyketide synthesis and catalyzes the transfer of modified CoA substrates. Five crystal structures have been determined, including those of ligand-free AcpS, complexes with CoA and acetyl-CoA, and two of the active site mutants, His110Ala and Asp111Ala. All five structures are trimeric and provide further insight into the mechanism of catalysis, revealing the first detailed structure of a group I active site with the essential magnesium in place. Modeling of ACP binding supported by mutational analysis suggests an explanation for the promiscuity in terms of both ACP partner and modified CoA substrates.

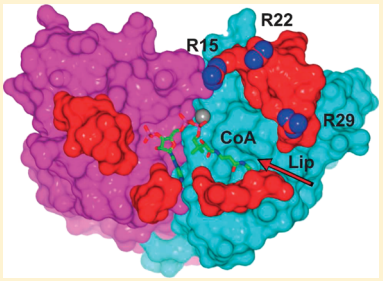

Phosphopantetheinyl transferases (PPTases) are essential for the biosynthesis of fatty acids, nonribosomal peptides, and polyketides.[1] Their function is to convert the apo form of a carrier protein into its active holo form by the post-translational addition of a coenzyme A (CoA)-derived phosphopantetheine (4′-PP) prosthetic group in a magnesium-dependent reaction[1,2] (Figure 1A). The thiol of this phosphopantetheine moiety is used as the covalent attachment site for intermediate acyl chains in fatty acid and polyketide biosynthesis. These acyl carrier proteins (ACPs) deliver the growing acyl chain to the various active sites of the synthase. This unique function means that the PPTases are of interest not only as possible targets for antibacterial agents[3,4] but also as tools for the selective derivatization of carrier proteins[5] and the specific labeling of proteins.[6]

The PPTases have been classified into three different groups. The bacterial group I or ACP synthase (AcpS)-like PPTases are ∼120 residues in length (Figure 1B) and act on the discrete ACPs from fatty acid or polyketide biosynthesis.[7] X-ray crystal structures of group I *Bacillus subtilis*,[8] *Streptococcus pneumoniae*,[9] *Vibrio cholera* [Protein Data Bank (PDB) entry 3H88, unpublished] and *Bacillus anthracis* (3HYK, unpublished) AcpSs reveal that this family adopts a trimeric quaternary structure, with the active site located in a cleft between the different subunits, resulting in three active sites per molecule. Group II is exemplified by the enzyme Sfp from *B. subtilis* that catalyzes the phosphopantetheinylation of the peptidyl carrier protein domain of bacterial surfactin synthetase.[10] Members of this group of enzymes are monomeric in structure but have two domains, with 2-fold pseudosymmetry within the monomer. To date, structures of the group II or Sfp-like PPTases from *B. subtilis*[11] and human[12] have been determined. The two domains in a group II monomer superimpose well on two subunits of the AcpS trimer with the active site in each lying between the two domains. The third group of PPTases exist as domains of yeast and fungal fatty acid and polyketide megasynthases.[13]

Several mechanisms for the phosphoryl transfer reaction have been proposed on the basis of the architecture of the active site of these structures. Whereas magnesium is essential for the activity of PPTases, bound calcium was observed in the reported AcpS structures.[8,9] By analogy to the coordination of the calcium ion, it was proposed that bound magnesium would play a direct role in the mechanism, activating a water that deprotonates a conserved serine in ACP (to which the 4′-PP group is ultimately attached).[8] An adjacent conserved aspartate on the ACP may also act as a base to remove this proton. Alternatively, for human Sfp where magnesium was present in the crystal structure, Glu191 was proposed to perform this role.[12]

To date, the only high-resolution information defining the interaction of ACP with any synthase component comes from AcpS and Sfp-like cocrystal structures with ACP.[8,12] Parris et al. cocrystallized a mutant *B. subtilis* AcpS in complex with ACP, demonstrating that the type II ACP and AcpS recognize one another through a series of negatively charged residues on helix II of ACP and reciprocal, positively charged residues on AcpS.[8] On the basis of single-point mutations, modeling, and nuclear magnetic resonance (NMR) studies, helix II is now widely

Received: March 11, 2011
Revised: May 19, 2011
Published: May 19, 2011

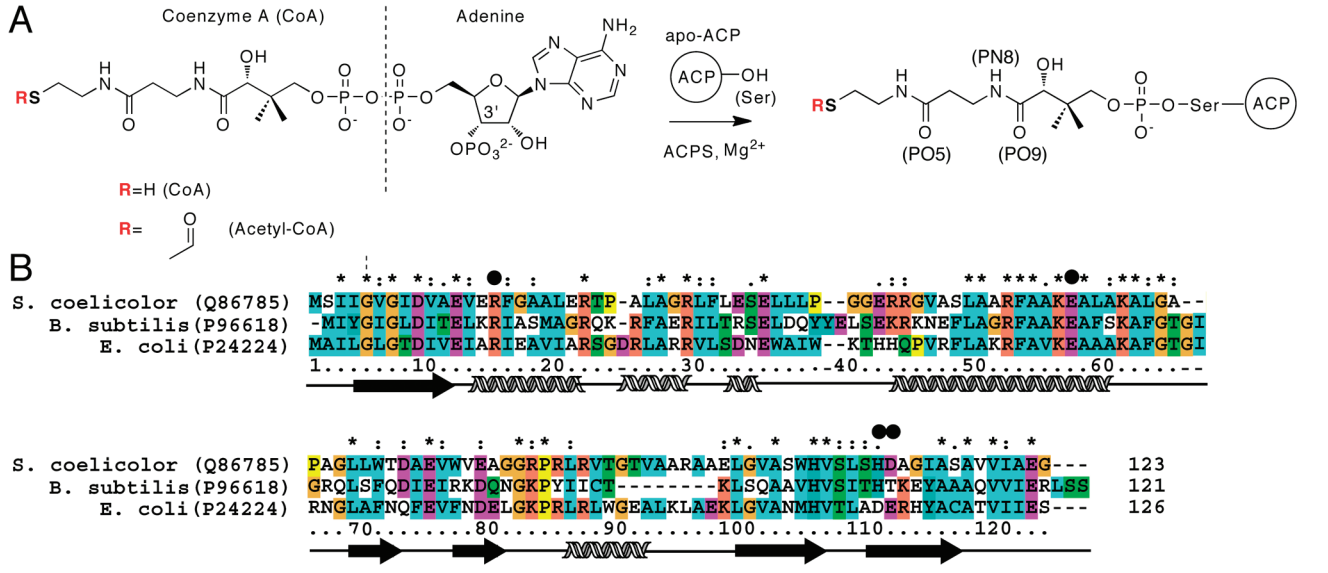

Figure 1. (A) Biosynthesis of holo-ACP from apo-ACP and CoA catalyzed by AcpS. The promiscuity of AcpS activity is shown where R on CoA may be substituted for an acyl group and subsequently transferred to the ACP along with the 4′-PP chain. (B) Alignment of type I AcpS sequences. Sequences were aligned with ClustalW. Secondary structure for *Sc* AcpS is indicated with arrows (β-strands) and rectangles (α-helix). The sequence numbering aligns with the *Sc* AcpS sequence (total of 123 amino acids), and the black circles highlight mutated residues R15, E57, H110, and D111.

believed to act as the universal recognition helix in type II ACP—protein interactions.[14−17] Sequence alignments reveal, however, that both fatty acid and polyketide type I ACPs have a lower overall negative charge. The crystal structure of the human type I fatty acid synthase (FAS) ACP bound to the Sfp-like PPTase revealed that although helix II was again involved in protein—protein interactions, the specificity may be governed by hydrophobic contacts and shape complementarity of the protein surfaces, rather than the presence of the correct hydrophilic pairs.

Streptomyces are the largest genus of actinobacteria and are responsible for the production of many biologically active natural products, including the polyketide actinorhodin (act).[18,19] The model *Streptomyces*, *Streptomyces coelicolor* (*Sc*), produces 22 secondary metabolites but encodes only three putative phosphopantetheinyl transferases, suggesting each one supports multiple biosynthetic pathways.[20] Two of these are Sfp group enzymes (SCO5883 and SCO667), and one is AcpS-like (SCO4744).[21] For example, no discrete phosphopantetheinyl transferase is associated with the actinorhodin polyketide synthase gene cluster, and SCO5883 and SCO667 were shown not to be essential for actinorhodin production. It has thus been suggested that SCO4744 (henceforth *Sc* AcpS), which is also essential for fatty acid biosynthesis, may play a dual role by phosphopantetheinylating both the fatty acid synthase and actinorhodin polyketide synthase ACPs in vivo.[22] *Sc* AcpS exhibits broad substrate specificity, can transfer phosphopantetheine onto the fatty acid ACP as well as onto both type I and type II polyketide synthase (PKS) ACPs, and can catalyze the transfer of the phosphopantetheinyl portion of a diverse range of acyl CoAs to ACP.[22] This property is important because it provides an entry point for a broad range of alternative building blocks into the synthetic cycle of both polyketides and fatty acids.

We have determined the crystal structure of *Sc* AcpS in the ligand-free form (at 2 Å) and in complex with magnesium and the substrates CoA and acetyl-CoA (both at 1.6 Å). Contrary to previous reports,[8] these models suggest that the transfer mechanism proposed for Sfp-like PPTases may be extended to the AcpS family. We present the results of a series of *Sc* AcpS mutants and two 1.4 Å structures of the active site mutants His110Ala and Asp111Ala whose effects on the activity of the enzyme can be explained in a structural context. We have performed binding studies with a range of ACP mutants that supports a modeled interaction of ACP with *Sc* AcpS. These studies provide a basis for explaining the promiscuity of *Sc* AcpS with respect to different ACPs and also with respect to acylated CoAs.

EXPERIMENTAL PROCEDURES

Expression and Purification of *Sc* AcpS. *Sc* AcpS was expressed and purified according to the method of Cox et al.[22] Briefly, *Sc* AcpS was cloned into the pET15b vector (Novagen) and expressed in *Escherichia coli* strain BL21(DE3). Expression was induced by isopropyl β-D-thiogalactoside (IPTG) over 5 h at 30 °C. Cells were harvested by centrifugation (5000*g* and 4 °C for 15 min) and lysed in buffer [50 mM Tris-HCl and 10 mM $MgCl_2$ (pH 8)]. *Sc* AcpS was purified by Ni^{2+} affinity chromatography (HisTrap HP, 5 mL, Amersham Pharmacia) followed by gel filtration (Superdex 75, Hi 16/60, Amersham Pharmacia). *Sc* AcpS was then transferred to storage buffer [50 mM Tris-HCl, 10 mM $MgCl_2$, and 10% (v/v) glycerol (pH 8)], concentrated to 10 mg/mL, and stored at −80 °C.

Expression and Purification of *S. coelicolor* ACP. Apo-ACP from the *S. coelicolor* fatty acid synthase or actinorhodin pathway was overexpressed in *E. coli* BL21(DE3) and was purified using an adaptation of the method developed by Crosby et al.[23] Harvested cells were resuspended in Tris-HCl buffer (50 mM, pH 8) and lysed by sonication. ACP was purified by anion exchange chromatography (HiLoad 26/10 Q-Sepharose, Amersham Pharmacia) [50 mM Tris-HCl (pH 8.5), 10 mM $MgCl_2$, 5 mM mercaptoethanol, and a 0 to 1 M NaCl gradient] followed by gel filtration [50 mM Tris-HCl (pH 8.5), 10 mM $MgCl_2$, 5 mM mercaptoethanol, and a 0 to 1 M NaCl gradient]. The fractions containing ACP were collected, desalted [50 mM Tris-HCl (pH 8.5), 10 mM $MgCl_2$, and 10 mM DTT], and stored

dx.doi.org/10.1021/bi2003668 |*Biochemistry* 2011, 50, 5704–5717

Table 1. Components of the Final Refined Models

component	ligand-free AcpS	ligand-bound AcpS	acetyl-CoA-bound AcpS	H110A AcpS	D111A AcpS
protein	residues 1−123	residues 1−123	residues 1−123	residues 1−123	residues 1−123
substrate (occupancy)	0	1 CoA (1.0)	acetyl-CoA (0.75) CoA (0.25)	1 CoA	2 CoA (0.5 each)
magnesium	0	1	1	1	2 (0.5 each)
other ions	1 sulfate	1 potassium	1 sulfate	1 sodium	1 sodium
water	residue 240	residue 183	residue 237	residue 237	residue 208
glycerol	1		1		

at −80 °C until they were required. Phosphopantetheinylation of apo-ACP to holo-ACP was achieved by incubation of purified apo-ACP (100 μM) with purified *Sc* AcpS (1 μM) and coenzyme A (1 mM) for 1 h, as described previously.[22]

Mutagenesis of ACP and *Sc* AcpS. The Stratagene QuickChange II Site-Directed Mutagenesis kit was used for the generation of the plasmids containing the desired point mutations (*Sc* AcpS, R15A, E57A, H110A, and D111A; *Sc* act PKS apo-ACP, D37A, D41A, D41E, and E47A; *Sc* FAS apo-ACP, E53A, D40A, E46A, and E52A). The only change to the protocol was the addition of DMSO during the polymerase chain reaction (PCR) for *Sc* AcpS mutants. The mutated plasmids were transformed into *E. coli* BL21(DE3) cells after being sequenced (Cogenics).

Crystallization, Data Collection, and Refinement. CoA or acetyl-CoA, at a final concentration of 5 mM, was added to 10 mg/mL purified protein, and the solution was left at 4 °C for 30 min and then centrifuged at 4 °C for 30 min (13000*g*). Crystals of the *Sc* AcpS−CoA−Mg^{2+} complex were obtained at 18 °C, from 0.3 M potassium thiocyanate (KSCN), 0.1 M sodium cacodylate (NaCac) (pH 6.5), and 15% PEG 4000. The best diffracting crystal of the *Sc* AcpS−acetyl-CoA complex was obtained in 0.2 M lithium sulfate, 25% PEG 2000 MME, and 0.1 M NaCac (pH 6.5), in the presence of 5 mM acetyl-CoA. The reservoir solution with 15% (v/v) glycerol was used as the cryoprotectant. The D111A mutant crystallized in 0.2 M KSCN, 0.1 M NaCac (pH 6.5), 8% PEG 20000, and 8% PEG 550 MME. These crystals were all cryoprotected using 15% glycerol and the reservoir solution conditions. The best data set for H110A was collected at station 10.1 in Daresbury, from a crystal obtained in 0.3 M sodium acetate, 0.1 M NaCac (pH 6.5), and 25% PEG 2000 MME with 10% PEG 400 as the cryoprotectant. Use of PEG 400 rather than glycerol was vital in this case for diffraction beyond 3.5 Å. The details of the components of the final refined models are listed in Table 1. Data processing was conducted using the HKL2000[24] and CCP4 suites of programs[25] (Table 2), and the same set of reflections was used for R_{free} throughout, extended from the set used in the original solution of the ligand-free structure.

The same crystal form was observed in all cases except for ligand-free AcpS, despite the range of conditions, with one protein subunit per asymmetric unit. In the ligand-free form, a trimer occupies the asymmetric unit, whereas in the ligand-bound form, the 3-fold axis of the trimer coincides with a crystallographic 3-fold axis so that there is one subunit in the crystallographic asymmetric unit. The ligand-free structure was determined by molecular replacement using Phaser[26] and the crystal structure of *B. subtilis* AcpS (PDB entry 1F7T) as a search model. ARP/warp[27−29] was unable to build the structure automatically into the initial electron density map, and 3-fold averaging with DM[30] was required to obtain a protein-like electron density map. ARP/wARP built 337 of 429 residues into this averaged map automatically. Further rounds of model building in Coot[31] and refinement with Refmac5[32] resulted in the final model. The ligand-bound structure was determined by molecular replacement with Phaser[33,34] using the ligand-free *Sc* AcpS structure as the search model, and the structures of the *Sc* AcpS−acetyl-CoA and *Sc* AcpS mutant−CoA complexes were determined using the protein component of the Mg^{2+}- and CoA-bound structure as a search model.

Generation of the *Sc* AcpS−ACP Complex Model. The NMR structures of *S. coelicolor* apo- and holo-actinorhodin PKS ACP (PDB entries 2K0Y and 2K0X respectively), as well as that of *E. coli* FAS ACP (PDB entry 1T8K), were used to study their possible interactions with AcpS.[35] The ACP structure closest to the geometric mean was chosen from each NMR ensemble. The *B. subtilis* AcpS−ACP complex (PDB entry 1F80) was used as a starting model.[8] A trimer of *Sc* AcpS was superimposed onto *B. subtilis* AcpS, while *S. coelicolor* ACP was superimposed onto *B. subtilis* ACP using secondary structure matching as implemented in COOT.[31]

Activity of AcpS Mutants. The mutant *Sc* AcpS was incubated with the *S. coelicolor* ACP using the 4′-PP transfer reaction conditions described above.[22] ACP was then purified by gel filtration, and the sample was subjected to mass spectroscopy to determine the percentage of the ACP that was successfully modified. A control reaction with wild-type AcpS was also conducted.

Isothermal Titration Calorimetery (ITC). The K_d values for wild-type and mutant *Sc* AcpSs and CoA or acetyl-CoA were determined by ITC. The protein and CoA were first dialyzed in ITC buffer [50 mM Tris-HCl (pH 8)]. A protein concentration of 8−10 μM and a substrate concentration of 120 μM were used. ITC was conducted using a VP-ITC microcalorimeter (MicroCal). A single experiment consisted of an initial injection of 7.5 μL of substrate solution into the cell containing the protein solution, followed by 18 other injections of 15 μL. The reaction was conducted at 25 °C, and each injection lasted for 30 s (15 for the first one) followed by a 240 s pause. For the identification of the weaker CoA binding site of *Sc* AcpS D111A, an initial CoA concentration of 1.5 mM was used. Fifteen injections of 2.5 μL of CoA over 5 s were followed by 15 other injections of 15 μL over 30 s. For each substrate or protein, the experiment was repeated at least three times. A blank that covered the concentration range of the appropriate CoA was run as a negative control in the absence of protein and was subtracted from experimental data. Alternatively, ΔH determined at the saturation of binding could be subtracted as this was determined to be linear from the control experiment.

Tryptophan Fluorescence Titration of ACP Binding to *Sc* AcpS. All assays were performed using a Spex Fluoromax

Table 2. Crystallographic Data Collection and Structure Refinement Statistics

	ligand-free	ligand-bound	acetyl-CoA	H110A	D111A
wavelength (λ, nm)	1.488	1.478	0.953	1.117	0.953
beamline	14.1, SRS Daresbury	10.1, SRS Daresbury	I02, Diamond	10.1, SRS Daresbury	I02, Diamond
resolution (Å)	50−1.98 (2.05−1.98)	50−1.62 (1.68−1.62)	50−1.56 (1.62−1.56)	50−1.35 (1.40−1.35)	50−1.4 (1.45−1.4)
space group	$P3_121$, $a = b = 75.94$ Å, $c = 108.35$ Å	$P2_13$, $a = b = c = 72.83$ Å	$P2_13$, $a = b = c = 72.83$ Å	$P2_13$, $a = b = c = 72.73$ Å	$P2_13$, $a = b = c = 72.83$ Å
no. of unique reflections	25759	16798	18659	28420	25707
completeness (%)	99.3 (95.7)	90.7 (69.3)	100 (100)	99.3 (99.3)	99.6 (96.4)
redundancy	6.4 (3)	6.1 (1.8)	9.4 (9.1)	9.3 (2.1)	7.9 (2.9)
$I/\sigma I$	22.19 (2.04)	18.9 (2.2)	32 (2.5)	32 (2.5)	34.7 (1.5)
R_{merge}	0.078 (0.378)	0.08 (0.33)	0.057 (0.381)	0.07 (0.22)	0.05 (0.51)
mosaicity (deg)	0.37	0.5	0.18	0.41	0.21
R_{free} (%)	0.220	0.21	0.232	0.205	0.21
R factor (%)	0.178	0.19	0.202	0.183	0.19
root-mean-square deviation for bond lengths (Å)	0.018	0.011	0.012	0.007	0.008
root-mean-square deviation for bond angles (deg)	1.690	1.417	1.533	1.229	1.271
% in most favored region in Ramachandran plot	98.1	99.2	97.8	100	100

spectrophotometer, at 25 °C in Tris buffer (50 mM, pH 7.3), $MgCl_2$ (10 mM), and glycerol [10% (v/v)]. The AcpS intrinsic tryptophan fluorescence was excited at 295 nm and measured over the range of 300−400 nm. AcpS (1 μM, 2 mL) was titrated with apo-ACP (200 μM stock) to a final ACP concentration of 5 μM. Interaction with ACP induces a quenching of the intrinsic tryptophan fluorescence of AcpS.

Mass Spectrometry. Phosphopantetheinylation of apo-ACP was confirmed using a MALDI-MS Voyager-DE STR Mass Spectrometer (Applied Biosystems). The mass spectra of acetyl-CoA used in the crystallization trials with AcpS were checked using a QStar XL mass spectrometer (Applied Biosystems) in positive ion mode. Samples were delivered using a Nanomate nanoelectrospray source (Advion) at a voltage of 1.3 kV and a gas pressure of 0.3 psi.

Accession Numbers. The structure coordinates for all five crystal structures have been deposited in the Protein Data Bank as entries 2JCA for ligand-free *Sc* AcpS at 2.0 Å, 2JBZ for *Sc* AcpS in complex with CoA at 1.6 Å, 2WDO for *Sc* AcpS in complex with acetyl-CoA at 1.5 Å, 2WDS for H110A in complex with CoA at 1.3 Å, and 2WDY for D111A in complex with CoA at 1.4 Å.

RESULTS

Crystallization of *Sc* AcpS. In the following descriptions, an amino acid numbering for *Sc* AcpS that includes a subunit position has been adopted; for example, SerA48 indicates Ser48 on subunit A. For the sake of clarity, we drop this notation when referring to point mutations. Wild-type and mutant *Sc* AcpSs were expressed and purified as described previously.[22] Wild-type *Sc* AcpS was crystallized as either the ligand-free form (no CoA present) or the ligand-bound form (with magnesium and CoA or with magnesium and acetyl-CoA). Two *Sc* AcpS mutants, His110Ala (H110A) and Asp111Ala (D111A), were also cocrystallized with CoA. The components and substrate stoichiometry present in the refined crystal structures are listed in Table 1. The crystallographic data collection statistics and refinement parameters are listed in Table 2. Magnesium was not visible in the electron density of the ligand-free form, despite being present in the crystallization buffer at a concentration of 10 mM. Both magnesium and CoA are present in a 1:1 ratio in wild-type and H110A *Sc* AcpS, but this ratio varied in both the acetyl-CoA and D111A forms. The structural basis for these observations is described below.

Fold and Oligomerization of *Sc* AcpS. The final models of the ligand-free and ligand-bound *Sc* AcpS were refined to crystallographic R factors of 17.8 and 19% and R_{free} values of 22 and 21%, respectively. In both forms, the *Sc* AcpS subunits associate to form a trimer (Figure 2A) with subunits we denote as A−C. Each subunit is comprised of five α-helices and five β-strands. Helix α4 forms the core of each subunit, packing centrally against a three-strand antiparallel β-sheet (β1, β4, and β5) on one side with the remaining helices on the other (Figure 2B). To form the trimer, the antiparallel β-sheets align around a 3-fold axis to form a nine-strand β-barrel with parallel interactions between the β-sheets, burying a total surface area of 4900 Å^2, or 1630 Å^2 per monomer. The Cα atoms of the three subunits in the ligand-free form can be superimposed with root-mean-square deviations (rmsd) of 0.55 Å (A on B), 0.72 Å (A on C), and 1.05 Å (B on C). Four flexible loops that lie in different conformations in the three different subunits and have higher B factors than the surrounding regions of structure can be identified. Mobile loop 1 (ML1, residues 21−26) joins α-helices 1 and 2, and loops 2−4 extend over residues 37−44, 65−70, and 79−82, respectively [ML2−4 (Figure 2B)]. The rmsd is improved to 0.29 Å (A on B), 0.39 Å (A on C), or 0.46 Å (B on C) when these areas are omitted. In the ligand-bound form, where the structure of each subunit is identical (through crystal symmetry), loops 1−4 are far less flexible and are displaced compared to their conformations in the ligand-free structure. This is demonstrated through well-defined electron density and B factors comparable to the average for all the main chain. This is in contrast to the ligand-free structure in

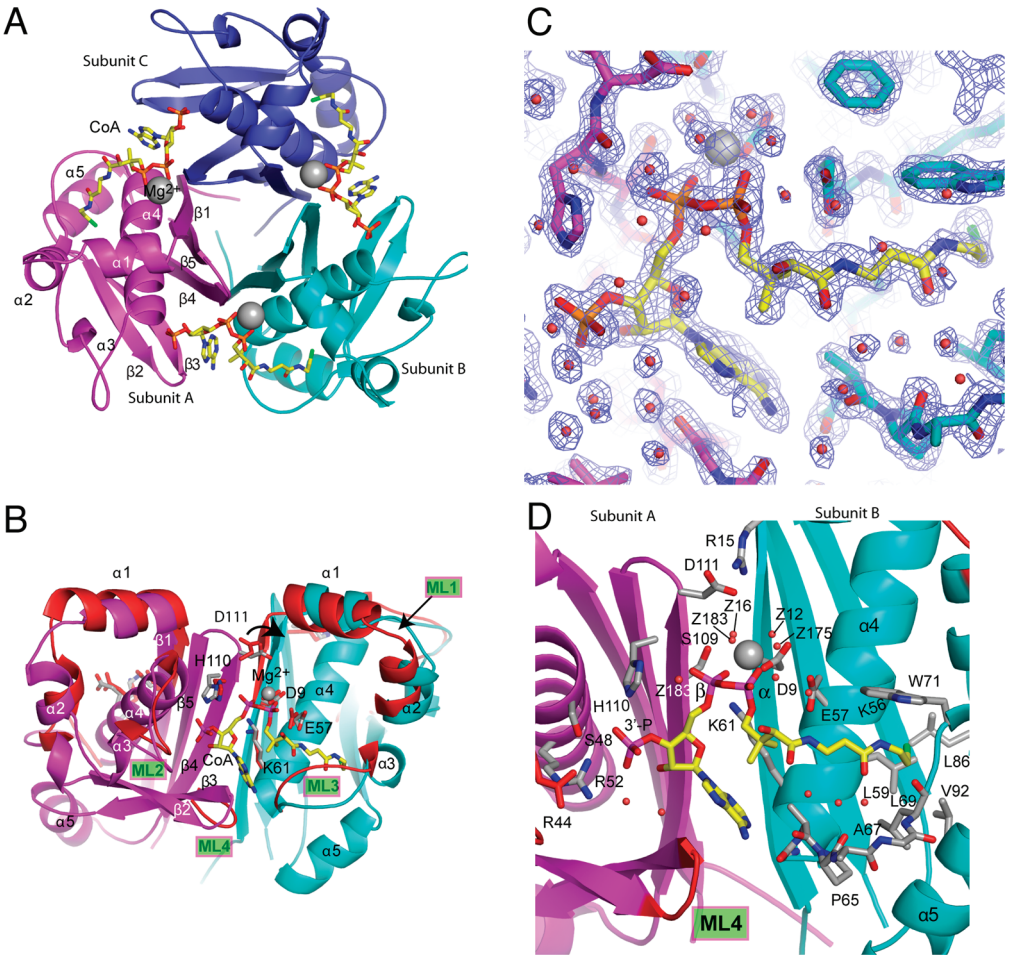

Figure 2. Structure of *Sc* AcpS. (A) Cartoon diagram of the trimer described above with Mg^{2+} represented as gray spheres and the CoA ligand shown in bond representation. In this figure and the following figures, subunit A is colored magenta, subunit B cyan, and subunit C blue. (B) Overview of the interface between subunits A and B, showing the mobile regions in the ligand-free structure (red) that undergo changes in conformation in the ligand-bound structure (magenta and cyan). The large displacement observed for Asp111 is indicated with an arrow. (C) CoA binding in the active site. Electron density from the final weighted electron density map is shown as a mesh contoured at 1.5σ. (D) Detailed view of the interface between subunits A and B. Important features of the model are shown as sticks (e.g., ML3), and carbons are colored magenta for subunit A, cyan for subunit B, and yellow for CoA.

which the final model has higher *B* factors compared to the main chain average and the electron density is less well-defined and varied between subunits.

CoA and Magnesium Binding Site. The active site and CoA binding site lie at the interface between two subunits, forming three identical active sites in the trimer (Figure 2A,B). The electron density for the active site, including the CoA, associated metal ion, and water ligands, is shown in Figure 2C and demonstrates the high quality of the data (see Figure S1 of the Supporting Information for the $F_o - F_c$ omit map). At each site, the adenine ring interacts with both subunits (Figure 2D) and binds in a pocket that is formed by a loop running into the N-terminus of helix 4 on subunit B and a loop between strands β2 and β3 of subunit A. The ribose is present in the 3′-*endo* conformation as observed in other AcpS structures.[8,9] The 3′-phosphate is held in place by interactions with residues HisA110, SerA48, and ArgA52 and with ArgA44 through hydrogen bonds provided by water molecules (Figure 2D). The α-phosphate interacts with magnesium, AspB9, and LysB61, while the β-phosphate, which is part of the leaving group in the transfer reaction, interacts with magnesium, the main chain of HisA110, and three water molecules (Z16, Z182, and Z183). In contrast, the phosphopantetheine arm interacts solely with subunit B and lies in a hydrophobic cavity between the central helix α4 and the small helix α5. At the entrance of the cavity, GluB57 makes a hydrogen bond to a backbone nitrogen of the phosphopantetheine side chain (PN8, Figure 1A), and AlaB65 and ProB66 in ML3 make water-mediated hydrogen bonds with the side chain carbonyl oxygens (PO9 and PO5, respectively). The hydrophobic cavity is composed of the aliphatic part of the LysB56 side chain and residues LeuB59, LeuB63, LeuB69, TrpB71, LeuB86, and ValB92.

Magnesium is essential for the activity of AcpS (Figure 1A) and is clearly visible in the electron density in the presence of CoA (Figure 2C). Its coordination sphere is composed of the oxygens of the α- and β-phosphates of CoA (with distances of 1.90 and 2.03 Å, respectively), the carboxyl group of AspB9 (2.12 Å), and three water molecules (Z12, Z16, and Z183 that coordinate to each other and are all within 2.16 Å of the Mg^{2+}). Z12 also interacts with the oxygens of the α-phosphate of CoA, AspB9, and water Z175. The second water (Z16) is also held in place by hydrogen bonds with the oxygens of the α-phosphate of CoA, the backbone of ValB10, and the side chain oxygen of

dx.doi.org/10.1021/bi2003668 |*Biochemistry* 2011, 50, 5704–5717

Table 3. Effects of Site-Directed Mutants of ACP on the Interaction with AcpS and the Efficiency of Phosphopantetheine Transfer (compared to C17S apo-ACP)

	K_d (μM)	activity (%)
Sc act PKS apo-ACP		
WT	1.1 ± 0.1	100
D37A	1.2 ± 0.1	0
D41A	7.0 ± 0.2	0
D41E	1.4 ± 0.1	15
L43A[a]	2.7 ± 0.1	15
L43R[a]	10.2 ± 0.2	0
E47A	1.8 ± 0.2	100
E53A	2.0 ± 0.1	75
D62A[a]	1.6 ± 0.1	20
D62N[a]	1.3 ± 0.1	86
Sc FAS apo-ACP		
WT	1.2 ± 0.2	100
D40A	9.2 ± 0.4	0
E46A	2.0 ± 0.1	100
E52A	2.2 ± 0.2	80

[a] From ref 37.

SerA109. The third water (Z183) is within hydrogen bonding distance of the oxygen of the α-phosphate, the side chain oxygen of AspA111, and water Z172 (not shown) from monomer A. GluB57 was not observed to be within coordinating distance of the Mg^{2+} ion (5.08 Å).

Comparison between Ligand-Free and -Bound AcpS. Superimposing trimers of ligand-free and -bound AcpS revealed several conformational changes (rmsd over Cα atoms of 0.94 Å) (Figure 2B). Most of these changes arise from the mobile loops in the ligand-free protein that are displaced in the bound form to accommodate binding of CoA. The backbone of ML1 and the final portion of helix 1 are displaced by 4−5 Å, while ML2, including ArgA44 in the 3′-phosphate binding pocket, also shows a significant 2 Å shift. ML3 from the B subunit moves to partially create the 4′-PP binding pocket, while ML4 orients to pack against the adenine base of CoA. In addition to the loop regions, there are also small concerted changes in the main chain around the CoA binding pocket that opens to accommodate the phosphopantethiene chain. The turn connecting β4 and β5 that contains AspA111 is also displaced up to 6 Å to cap off the magnesium binding site and allow coordination with the magnesium-bound water (Z183). The side chain of TrpB71 also rotates by approximately 30° to create the pocket in which the tip of the phosphopantethiene chain is buried (Figure 2D).

Activity and CoA Binding of Active Site Mutants. Mutational studies of the human group II Sfp-like PPTase have previously highlighted the possible mechanistic roles of H111, Q112, and E181 (equivalent to HisA110, AspA111, and GluB57, respectively, in this study (Figure 1B)).[12] E181 has been shown to play an important role in Mg^{2+} binding. This residue is also thought to play a vital mechanistic role, deprotonating the active site serine of the ACP. The histidine (H111) in the human group II enzyme was also shown to be important for Mg^{2+} and CoA binding. The influence of a Q112 mutation on Mg and CoA binding was negligible, though a significant reduction in k_{cat} was observed and in the human enzyme it was not clear how this influence was exerted. The structure of *B. subtilis* AcpS also highlighted the roles of positively charged residues, including R14, which was thought to lock the Asp of the conserved DSL motif of the ACP in the correct conformation for 4-phosphopantetheinyl transfer. No mutational studies were reported to confirm this. Therefore, we made four *Sc* AcpS mutations as well as nine mutations to *Sc* act PKS apo-ACP and three to *Sc* FAS apo-ACP: *Sc* AcpS E57A to confirm its mechanistic role, H110A to clarify its influence on CoA binding and/or mechanism, and D111A to determine its longer-range influence on the active site. We have also mutated ArgB15 (R15A) and the reciprocal negatively charged residues on act ACP (see Table 3 and Figure 2D). All of the mutants were cloned, overexpressed, sequenced, and purified using a protocol identical to that of wild-type *Sc* AcpS. The ability of the mutant AcpS to bind CoA and phosphopantetheinylate ACP was then assessed.

The affinity of CoA for the wild-type and mutant proteins was measured by ITC (Table 4 and raw data shown in Figure S2 of the Supporting Information).[36] For wild-type AcpS, a 1:1 stoichiometry was determined for CoA (one CoA per active site of the trimer) with a K_d of 0.38 μM. Essentially, the H110A mutant gave results similar to those of the wild-type enzyme. R15A also exhibited a K_d comparable to that of the wild type but with a much reduced enthalpy of binding. The rather poor response of R15A by ITC led us to corroborate these data using intrinsic tryptophan fluorescence quenching (ITF). WT AcpS gave a K_d for CoA of 0.75 μM that agreed with the ITC data, while R15A showed a clear 3-fold reduction in the level of CoA binding. For the E57A mutant, the K_d for CoA was determined to be 4−6-fold weaker than that of the wild type by ITC and ITF. The binding of CoA to the D111A mutant was, however, more complex. The initial titration revealed the presence of a strong binding interaction with a stoichiometry of 0.5 ± 0.1 indicating the active sites of the trimer were not fully occupied. In a second experiment, however, after initial saturation with CoA, the titration was continued by further loading at a very high concentration of CoA (2.5 mM). In this second experiment, a weaker binding site was detected. Because of the large difference in enthalpy between the two binding sites, it was not possible to determine accurately the K_d for the second binding site.

Wild-type AcpS converted 100% of apo-ACP to holo-ACP as confirmed by ESMS. The four *Sc* AcpS mutations described above had reduced activity (Table 4). Despite a CoA binding profile similar to that of the wild type, the activity of H110A was reduced 20-fold. D111A and R15A exhibited ∼30 and 15% activity, respectively, while E57A was completely inactive.

Structure of the H110A *Sc* AcpS Mutant. The profound effect on the activity of H110A despite a negligible loss of CoA binding led us to structurally characterize this mutant. The overall structure of the H110A mutant AcpS−CoA complex is very similar to that of the wild-type *Sc* AcpS−CoA complex with a rmsd of Cα atoms after superimposition of 0.22 Å. There is well-defined electron density for an alanine in place of histidine at position 110, and a water molecule in the position previously occupied by the NE2 atom (Figure 3A). The main chain is displaced by 0.5−0.6 Å from residue 110 to 113, which moves the side chain of Asp111 by 1.3 Å. In this position, the side chain carboxylate of AspA111 no longer makes a hydrogen bond with the water equivalent to Z183 that ligates magnesium. Instead, AspA111 forms a new intersubunit hydrogen bond with the side chain of ArgB15. The direct coordination sphere of the magnesium and the CoA binding site remains essentially unchanged with the exception of minor changes in atomic positions. However, we

Table 4. Binding affinity for the ligand-bound AcpS and the acetyl-CoA AcpS determined by ITC and ITF

	ITC			ITF	
	K_d (μM)	n	ΔH (cal/mol)	K_d (μM)	activity (%)
WT AcpS−CoA	0.38 ± 0.02	1.2 ± 0.1	−4000 ± 400	0.75 ± 0.04	100
R15A AcpS−CoA	0.8 ± 0.2	1.0 ± 0.2	−1030 ± 200	2.29 ± 0.31	15
E57A AcpS−CoA	2.5 ± 1.6	1.17 ± 0.14	−2500 ± 450	3.64 ± 0.21	0
H110A AcpS−CoA	0.45 ± 0.07	0.98 ± 0.05	−3500 ± 400	not determined	5
D111A AcpS−CoA	0.85 ± 0.04	0.5 ± 0.1	−7000 ± 1800	not determined	28
WT AcpS−acetyl-CoA	2.4 ± 0.1	0.94 ± 0.07	−1600 ± 200	not determined	100[a]

[a] Based on 100% conversion over the course of the assay.[22]

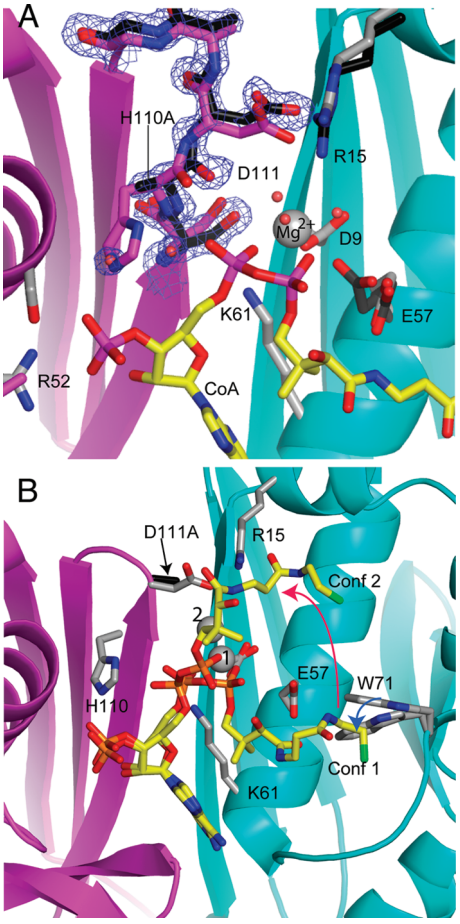

Figure 3. Structural comparison of *Sc* AcpS with the H110A and D111A structures. (A) Superposition of selected regions of the H110A mutant with the wild-type *Sc* AcpS structure. The interface of subunit A (magenta), subunit B (cyan), and bound CoA (yellow) of wild-type *Sc* AcpS is shown, and residues surrounding the histidine mutation in the H110A structure (black) are superimposed. Electron density for the H110A mutant from the final weighted electron density map is shown in mesh, contoured at 1.2σ. Water molecules from the mutant structure are shown as red spheres. (B) Cartoon diagram of the subunit A−subunit B interface of wild-type *Sc* AcpS colored as in panel A. Selected side chains of the D111A mutant are colored black, and the two conformations of CoA observed in this mutant are colored yellow. The magnesium ion (gray) is labeled 1 or 2 corresponding to each conformation of the CoA. In conformation 2, CoA moves away from the binding region observed in the WT enzyme (indicated by the red arrow) and Trp71 moves to occupy the residual cavity (blue arrow).

were able to detect two conformations for GluB57. In the first, GluB57 shows a conformation similar to that of wild-type AcpS and does not participate in Mg^{2+} binding. In the second, a rotation around the Cα−Cβ bond allows this residue to partially participate in coordinating the magnesium. The electron density around the β-phosphate also indicates that there is more conformational variability than in the wild-type structure, whereas the position of the rest of the CoA moiety is more precisely defined.

Structure of the D111A *Sc* AcpS Mutant. Similar to H110A, D111A had significant effects on activity but not CoA binding. The structure of the D111A mutant was almost identical to that of wild-type ligand-bound *Sc* AcpS with an rmsd of Cα atoms of 0.2 Å. However, the CoA is observed to bind in two distinct conformations, one of which is similar to the wild-type conformation, with the magnesium binding site also conserved (Figure 3B, conformation 1). In the second conformation, however, the phosphopantetheine chain of CoA extends up along the subunit interface over the surface of *Sc* AcpS close to ArgB15 in the B subunit (Figure 3B, conformation 2). In this conformation, the side chain of TrpB71 rotates by approximately 30°, moving 3 Å at the tip, filling up the empty CoA binding pocket by adopting a conformation similar to that observed in the ligand-free structure. In this case, the associated magnesium ion is shifted by 2 Å.

Binding and Activity Measurements of PKS/FAS ACPs and *Sc* AcpS. *Sc* AcpS is able to modify both the *S. coelicolor* apo-FAS ACP (*Sc* FAS ACP) and actinorhodin polyketide apo-ACP (*Sc* PKS ACP).[22] To test whether these ACPs interact with *Sc* AcpS using a common binding motif, a range of analogous *Sc* FAS and PKS ACP mutants were prepared. These mutations included the aspartate of the highly conserved DSL motif (FAS D40A and PKS D41A/D41E), residues in helix II (FAS E46A/E52A and PKS E47A/E53A), and a conserved aspartate in the long loop preceding helix II (PKS D37A). Fluorimetric titrations were used to determine dissociation constants between the ACP variants and *Sc* AcpS (Table 3). In these assays, an observed stoichiometry of 1:1 confirmed that three ACPs bound to the AcpS trimer. No evidence to suggest co-cooperativity in binding was found, and the binding sites appear to behave independently. *S. coelicolor* PKS and FAS ACPs bind to *Sc* AcpS with very similar dissociation constants (K_d) of 1.1 ± 0.05 and 1.2 ± 0.15 μM, respectively. The majority of the mutants showed very moderate changes (<2-fold) in dissociation constants, consistent with them lying at the ACP−AcpS interface but not making strong individual contributions to the overall binding energy. The D40A *Sc* FAS ACP and D41A *Sc* act PKS ACP mutants, however, showed an almost one order of magnitude reduction in binding affinity with

dx.doi.org/10.1021/bi2003668 |*Biochemistry* 2011, 50, 5704–5717

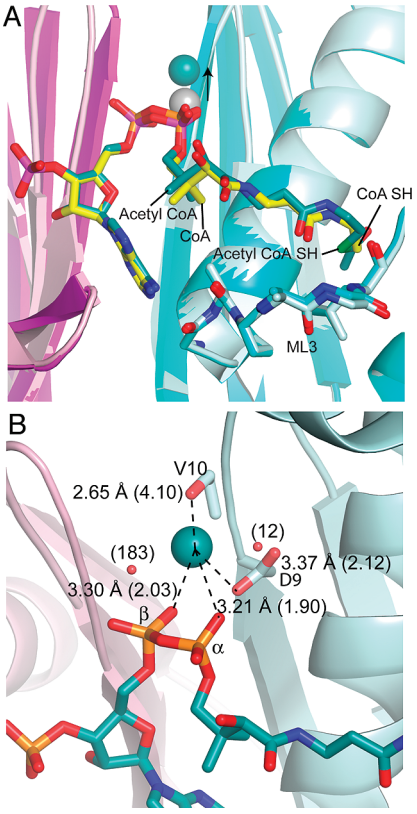

Figure 4. (A) Comparison of CoA and acetyl-CoA (in bond representation) binding at the interface of *Sc* AcpS. For the CoA-bound form, subunit A is colored magenta and subunit B cyan, and they are colored pink and blue/gray, respectively, in the acetyl-CoA structure. The CoA carbon backbone is colored yellow and the acetyl-CoA blue. (B) Coordination of the Mg^{2+} in the acetyl-CoA-bound form. Distances from AcpS and acetyl-CoA to Mg^{2+} are indicated by dotted lines, and the corresponding distances in the CoA-bound form are shown in parentheses.

their K_d values increased to 7.0 ± 0.2 and 9.2 ± 0.4 μM, respectively. D41E and D37A *Sc* PKS ACPs show ACP:AcpS binding ratios almost identical to that of the wild type. A reciprocal mutation on AcpS, R15A, was also tested for ACP binding. Similar to the single-point mutations on ACP, R15A gave a K_d value comparable to that of the wild type (0.5−1.0 μM). E57A, which is also close to the ACP binding site, exhibited an interaction comparable to that of the wild type (1.0 μM).

The ability of the ACP mutants to act as substrates for AcpS was assayed by incubating ACP and CoA with a catalytic amount of AcpS and monitoring phosphopantetheinylation by mass spectrometry. The D40A *Sc* FAS ACP and D41A *Sc* PKS ACP mutants were inactive. Surprisingly, the D37A and D41E mutants, which had no effect on ACP binding, showed 0 and 15% activity, respectively. The remaining mutants retained almost full activity (≥75%) (Table 3). Point mutations of L43 and D62 in *Sc* act PKS ACP have been reported previously and are included for comparison.[37]

Analysis of the Crystal Structure of *Sc* AcpS in Complex with Acetyl-CoA. Electron density in the CoA binding pocket of the AcpS−acetyl-CoA complex structure showed evidence of occupancy predominantly by acetyl-CoA, with a smaller proportion of CoA. Difference electron density maps were used to gauge the correct occupancy for both substrates, by trying to minimize the positive and negative density, resulting finally in 75% occupancy for acetyl-CoA and 25% occupancy by CoA.

The structure of the acetyl-CoA−AcpS complex is very similar to that of the CoA−AcpS complex (Figure 4A). The rmsd after Cα superimposition of these two species is 0.20 Å. The electron density for the acetyl-CoA is clear and includes the extra acetyl group. Acetyl-CoA adopts a slightly less extended conformation than CoA, so that the acetyl group lies in a position similar to that of the terminal sulfur of CoA. ML3 of subunit B changes conformation to partially accommodate the more compressed pantetheine arm beside which it lies. The maximal displacement is 0.5 Å for the main chain atoms of GlyB68 in the center of ML3. In the holo structure, the magnesium ion is coordinated to both α- and β-phosphates of CoA (with distances of 2.03 and 1.90 Å, respectively), to the carboxyl group of AspB9 (2.12 Å), and to three water molecules (all within 2.16 Å) (Figure 4B). In the acetyl-CoA structure, however, the magnesium is displaced by 1.9 Å and lies 3.21 and 3.30 Å from the α- and β-phosphates, respectively, and 3.37 Å from AspB9 (vs 1.90, 2.03, and 2.12 Å, respectively, in the AcpS with CoA bound). In addition, the ion remains coordinated to waters equivalent to Z12 (2.87 Å) and Z183 (3.10 Å distant), but the equivalent to water Z16 is missing. The magnesium is now positioned 2.65 Å from the main chain oxygen of ValB10 and 3.17 Å from the carboxyl group of AspA111 in the small loop connecting β4 and β5. The electron density for the small loop containing AspA111 was not clear, however, and both ligand-free and bound forms of this loop were observed.

The affinity of acetyl-CoA for *Sc* AcpS was measured by ITC (Table 4 and raw data shown in Figure S2 of the Supporting Information). Acetyl-CoA exhibited a 6-fold reduction in binding affinity (2.4 μM) and a concomitant 2-fold loss in binding enthalpy but maintained the 1:1 binding ratio. This value is in reasonable agreement with the K_M of 25 μM determined for acetyl-CoA with human PPTase and ACP.[12] The overall reduction in binding affinity does, however, agree with the observed compression and displacement of the CoA as well as the imperfect coordination of the magnesium ion.

DISCUSSION

The high-resolution crystal structure of the *Sc* AcpS reveals that it adopts a trimeric structure. The structures of the FAS *B. subtilis* group I ligand-bound AcpS (with CoA and Ca^{2+}),[8] *St. pneumoniae* AcpS (with 3′,5′-ADP and no catalytic metal ion),[9] *V. cholerae* AcpS (with CoA and Mg^{2+}, unpublished), and *B. anthracis* AcpS (with 3′,5′,ADP, unpublished) have all been reported and show a similar trimeric arrangement with the active site situated at the interface between adjacent subunits. These four models were superimposed on the ligand-bound *Sc* AcpS and found to give a rmsd range of 1−2 Å between the Cα atoms. The overall fold of each structure was remarkably similar considering that the maximal level of sequence identity is only 27%. The secondary structure is also conserved with the exception of helix α5, which is only present in the *S. coelicolor* and *V. cholerae* structures. In the corresponding region of the *B. subtilis* crystal structure, a PCR error resulted in the mutation of a glutamine to proline,[8] which would preclude the formation of this helix.

Comparison with *B. subtilis* AcpS. Panels A and B of Figure 5 compare the regions that surround the active site and interact with CoA in *Sc* and *B. subtilis* AcpS. ML4, which interacts with the adenine base at one end of the CoA, is in a similar conformation in all of the structures, and overall, the 3′-phosphate, ribose, and

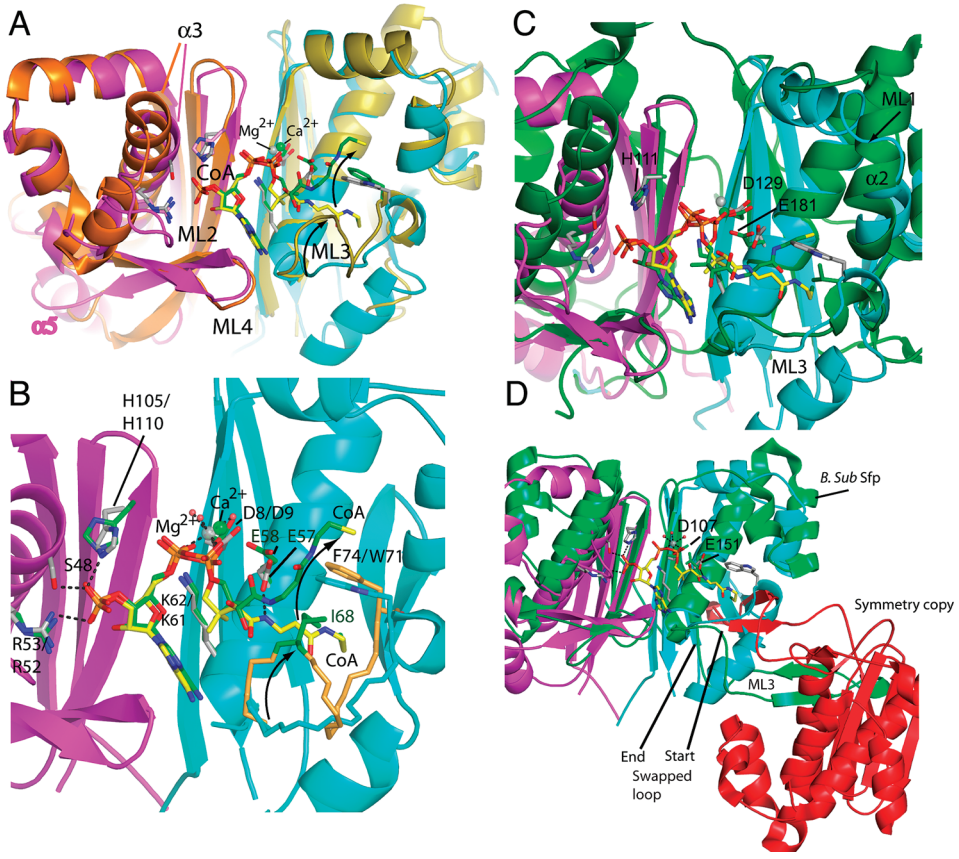

Figure 5. Structural comparison with other phosphoryl transferases. (A) Active site comparison between *Sc* and *B. subtilis* AcpS. *Sc* AcpS subunit A is colored magenta and subunit B cyan. *B. subtilis* subunit A is colored orange and subunit B gold. CoA and side chains are shown in bond representation with carbon atoms colored yellow for *Sc* and green for *B. subtilis* ACPS. Magnesium is colored gray, and calcium is shown as a green sphere. The displacement of ML3 is indicated by an arrow, and the displacement of the 4′-PP side arm above F74 in *B. subtilis* (green sticks) can be clearly seen. (B) Expansion of the active site showing in detail the CoA binding mode in *Sc* and *B. subtilis* AcpS. Shading the same as in panel A and sequence numbering is shown as *B. subtilis* AcpS / *Sc* AcpS. (C) Superposition of the dimer interface in *Sc* (magenta and cyan with CoA colored yellow) with the human Sfp-like PPTase (green). (D) Superposition of the dimer interface of *Sc* AcpS (magenta and cyan with CoA colored yellow) with *B. subtilis* sfp (protein colored green) and the adjacent symmetry-related molecule in the crystal lattice colored red.

adenine base of CoA superimpose well (Figure 5A). The mobile loop, ML2, that is present in the *Sc* AcpS adjacent to the 3′-phosphate is missing from the *B. subtilis* structure. Instead, this stretch of amino acids is incorporated into a longer helix α3. A sequence comparison shows *Sc* AcpS has a proline in this stretch that is not found in the other structures and most probably explains why helix α3 is disrupted. Despite these structural differences, however, the 3′-phosphate is oriented similarly in the two structures. Important differences, however, are observed at the catalytic site surrounding the diphosphate pair that is cleaved in the transfer reaction. In *Sc* AcpS, a magnesium ion is ligated by these phosphates, whereas in *B. subtilis* AcpS, a calcium ion was observed in the binding site.[8] The Ca^{2+} coordination sphere includes AspB8, an oxygen from the α-phosphate of CoA, and three water molecules as in *S. coelicolor*, but rather than the β-phosphate providing an oxygen ligand, the side chain of GluB58 provides the sixth ligand. This results in a different conformation of the β-phosphate, GluB58, and the phosphopantethiene chain. This is consistent with the observation that calcium allows catalysis in the *B. subtilis* enzyme but only at a much reduced rate.[8] The importance of the α- and β-phosphates of CoA in ligating the Mg^{2+} is also highlighted by our observation of no Mg^{2+} binding in the ligand-free form of *Sc* AcpS.

In the *S. coelicolor* structure, the phosphopantetheine chain (yellow in Figure 5A,B) is buried in a hydrophobic pocket, whereas in the *B. subtilis* AcpS, it extends over the surface of the B subunit (green). In *Sc* AcpS, ML3 forms the side of this pocket but the loop shows a very different conformation in *B. subtilis* AcpS. Here the loop is displaced upward (indicated by an arrow in Figure 5A,B), and Ile68 (green in Figure 5B) now occupies this binding pocket forcing the 4′-PP out across the surface of the protein. In the case of *B. subtilis*,[8] it was suggested that this portion of the structure must move to accommodate the ACP. In the *Sc* AcpS structure, a similar conformational change occurs upon CoA binding.

Comparison with Other Group I AcpSs. Further detailed analysis of the structural differences between the other AcpS structures is complicated by the lack of consistency in the bound cofactors and substrates as detailed above. The 3′,5′-ADP-bound *St. pneumoniae* and *B. anthracis* AcpS structures lack a 4′-PP chain leading to a vacant 4′-PP binding pocket that is filled by ML3. Finally, although the *V. cholerae* AcpS crystal structure contains CoA, it has only a single Mg^{2+} ion per trimer and displays a variety of conformations.

Comparison between *Sc* AcpS and Dimeric Group II Phosphotransferases. Human PPTase[12] belongs to the group

dx.doi.org/10.1021/bi2003668 |*Biochemistry* 2011, 50, 5704–5717

II phosphotransferase family, a group that is represented by the Sfp protein from *B. subtilis*.[11] While *Sc* AcpS has 123 residues, the human enzyme is longer, containing 315 amino acids. In addition, all group II enzymes show a trimeric arrangement, while the Sfp-like PPTase group is characterized by a two-domain architecture, joined by a linker region. Each domain is similar to a single group I subunit, and the proteins can be superimposed using secondary structure matching. Human PPTase, however, has longer N- and C-termini in comparison to those of the *S. coelicolor* protein. The superimpositions between *Sc* AcpS and human and *B. subtilis* Sfp-like PPTases are shown in panels C and D of Figure 5, respectively. In the human Sfp-like PPTase, CoA and magnesium are located at the interface between the two Sfp domains, with the ribose in the same 3′-*endo* conformation (Figure 5C), while the 3′-phosphate of CoA is salt-bridged to His121, analogous to HisA110 in *Sc* AcpS. The adenine rings of the CoAs are also bound in a similar way with the exception that the cleft is wider in the human PPTase. In the human PPTase, ML1 is substituted with a longer α-helix (analogous to the shorter α2 in *Sc* AcpS), while ML3 shows a small upward displacement into the phosphopantetheine binding pocket. The phosphopantetheine chains are also bound in different conformations with the two terminal thiols 6 Å apart. The human phosphopantetheine arm is located in a hydrophobic outer shell,[12] which is smaller than the *S. coelicolor* cavity. At the catalytic center of the human model, the magnesium ion is once again coordinated to the two phosphates of CoA, a water molecule, an aspartate (Asp129), equivalent to AspB9 of *Sc* AcpS, and a glutamate residue, Glu191 (equivalent to GluB57 of *Sc* AcpS). An equivalent coordination pattern is observed in the *B. subtilis* Sfp structure (Figure 5D, Asp107 and Glu151). Both coordination shells closely match those observed in *Sc* AcpS, the exception being that GluB57 does not coordinate Mg^{2+} in *Sc* AcpS.

The region equivalent to ML3, however, shows greater variability between the various structures. *S. coelicolor* and human ML3 conformations are comparable (Figure 5C), whereas this region protrudes from the molecule in the crystal structure (PDB entry 1QR0) of the *B. subtilis* Sfp (Figure 5D, green). A comparison, however, to both the human PPTase and the trimeric AcpSs suggests that this is an artifact of crystallization due to domain swapping of the ML3 hairpin with an adjacent symmetry-related molecule in the crystal lattice (Figure 5D, red). *B. subtilis* Sfp is likely to adopt a compact binding site similar to those observed in the AcpS structures rather than the extended one implied by the monomeric crystal structure observed in isolation because the equivalent loop from a symmetry-related molecule completes the compact globular structure.

Proposed Reaction Mechanism. The complex active site architecture of the AcpS ensures that the catalytic magnesium, CoA, and ACP are brought together in the correct orientation for 4′-PP transfer to occur. The sequential nature of the mechanism makes interpretation of point mutations complex as their effects may originate from a loss of catalytic efficacy, poor cofactor or substrate binding, loss of active site structural integrity, or a combination of these factors. For example, unexpectedly, we observed two alternate CoA binding conformations in the D111A mutant by X-ray crystallography, and the difference between wild-type and mutant ITC data may be interpreted as being due to the presence of a second, weakly bound CoA in a nonproductive conformation in the mutant. AspA111, therefore, appears to exert a long-range ordering effect on the active site by acting as a gatekeeper for the phosphopantetheine chain. Only one conformation would be expected to be catalytically active and overlap directly with the proposed ACP binding site.[8]

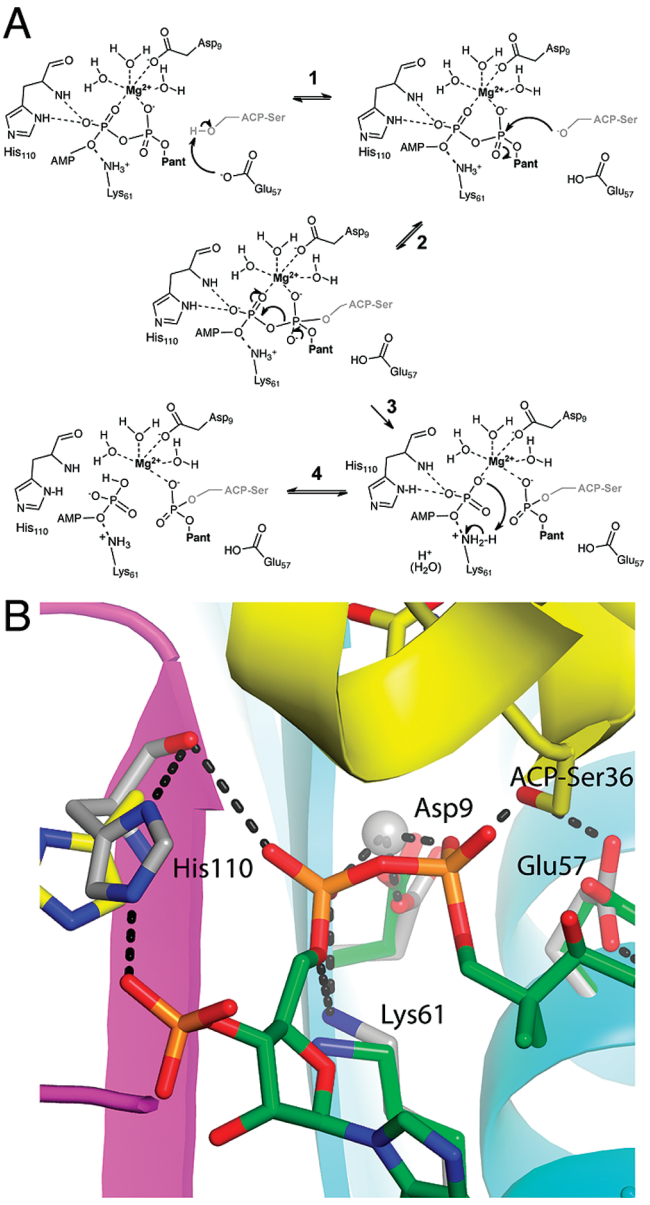

Figure 6. Proposed reaction mechanism for phosphopantetheinyl transfer in *Sc* AcpS and model of bound ACP. (A) The transfer mechanism is divided into four steps. In step 1, GluB57 abstracts a proton from the hydroxyl group of the conserved serine on ACP (light gray). In step 2, the alkoxide anion attacks the β-phosphate of CoA. In step 3, cleavage of the phospodiester bond leads to the transfer of negative charge to the oxygen of the α-phosphate coordinating the Mg^{2+}. In step 4, reprotonation of the α-phosphate could occur from LysB61 or potentially HisA110 followed by dissociation of the complex. (B) Model of *B. subtilis* ACP in the active site of *Sc* AcpS generated by superposing the complex structure of *B. subtilis* ACP AcpS on the structure of *Sc* AcpS. ACP is colored yellow; *Sc* AcpS is shown with the A subunit colored magenta and the B subunit cyan, and selected side chains are shown from *B. subtilis* AcpS with carbons colored forest green as in Figure 5. Dotted lines represent hydrogen bonds observed in the crystal structure of *Sc* AcpS and potential interactions in the case of bonds shown between *B. subtilis* ACP and *Sc* AcpS.

dx.doi.org/10.1021/bi2003668 |*Biochemistry* 2011, 50, 5704–5717

By analogy with the human and *B. subtilis* group II class of PPTases, we suggest that GluB57 acts as the catalytic base that extracts a proton from the conserved serine of ACP (step 1). The positive helix dipole moment and proximity to the cationic Mg^{2+} may lower the pK_a of serine to allow this to take place. GluB57 is conserved in both group I and II PPTases. Mutation of this residue to an alanine has been shown to reduce the level of catalysis by 3 orders of magnitude (Figure 6A, step 1).[12,38] In these studies, as well as acting as a base, the glutamate also partially coordinates the Mg^{2+}. This dual role has not been established in the *Sc* AcpS as there is no apparent coordination to the magnesium. For the *B. subtilis* AcpS, it was proposed that Asp35 acts as a general base, deprotonating a water molecule that then removes the hydroxyl hydrogen from Ser36.[8] This alternate mechanism was suggested as GluB58, analogous to GluB57, was involved in the coordination of the bound Ca^{2+} and presumed to be unable to deprotonate the serine. Figure 6B shows a superposition of the *B. subtilis* holo-ACP with *Sc* AcpS in the vicinity of the active site. The phosphopantetheine side chain has been truncated back to serine, but no other adjustments have been made to the superposition described in Experimental Procedures. While the geometry is not perfect, GluB57 is within hydrogen bonding distance of the ACP serine (Ser36 in *B. subtilis*) and the oxygen of the serine lies ~2 Å from the phosphate, which it must attack in the transfer reaction. Small adjustments to the position of the serine could place it in an optimal position for in-line attack on the phosphate while maintaining the interaction with the glutamate (Figure 6A, step 2).

The correct presence of Mg^{2+} in the active site reveals that GluB57, in the unbound form of AcpS, does not coordinate the metal cation and is available to deprotonate the serine of the ACP. However, the observation of at least partial coordination in the H110A structure suggests that this residue has the capacity to undergo minor conformational changes and the coordination shell of the Mg^{2+} ion can change to accommodate this. This could occur, for example, upon ACP binding. Nonetheless, either scenario presents an active site architecture and transfer mechanism that are closely in line with those suggested for the group II PPTases.

Once deprotonated, the serine hydroxide group can attack the β-phosphate of CoA in an addition−elimination reaction.[39] Following this, the final steps of the transfer are similar to those outlined in detail for the group II PPTases. The active site architecture suggests a mechanism by which magnesium has a role in catalysis through stabilizing the resulting negatively charged 3′,5′-ADP after the transfer of the 4′-PP group and not simply a role in CoA binding (Figure 6A, step 3). Our structural and mutational results support the role of HisA110 in stabilizing negative charge transfer. Although HisA110 is involved in a salt bridge with the 3′-phosphate of CoA, mutation of this residue affects only catalytic activity, not CoA binding affinity. The structure of the alanine mutant indicates that the CoA binding site is not perturbed, with hydrogen bonding interactions preserved through changes in the water network. In the human and Sfp PPtase, mutation of the analogous histidine differed in showing reduced affinity for both CoA and magnesium. In these cases, it was clearly not possible for water molecules to provide an alternate hydrogen bonding network for proton transfer or HisA111 simply had a much greater role in CoA binding. Lastly, LysB61 (as suggested from the human group II PPTase[12]), or possibly HisA110, is positioned to be able to protonate the negatively charged phosphate group followed by dissociation of the complex (Figure 6A, step 4).

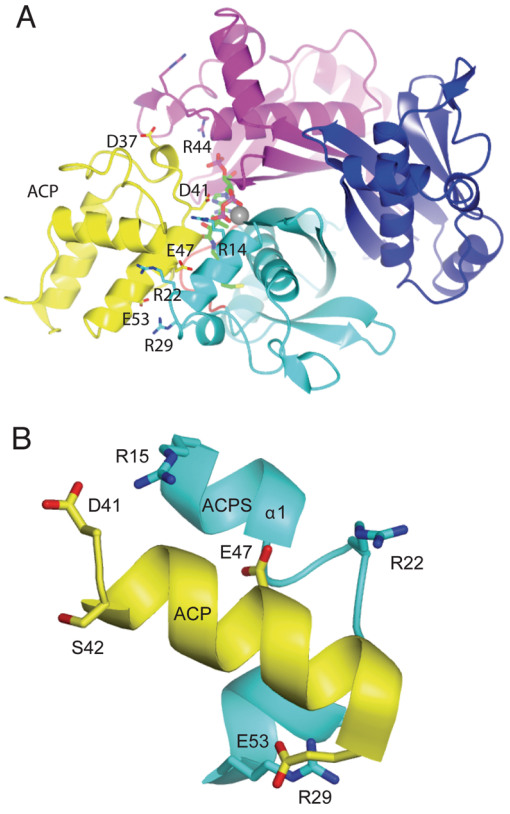

Figure 7. (A) *Sc* AcpS trimer shown in cartoon representation as before, with the *S. coelicolor* ACP model shown in cartoon representation in yellow. (B) Helix 1 from subunit B of *Sc* AcpS colored cyan and helix 2 of *S. coelicolor* ACP yellow, with conserved side chains shown in bond representation.

Interaction between ACP and AcpS. The ternary complex between *B. subtilis* AcpS and ACP revealed that three ACPs bind to the trimer[8] whereas a single ACP binds to the didomain human group II PPTase.[12] Both give an overall protein stoichiometry of 1:1, although clearly in the case of the group II PPTase there is one ACP per two domains. In both cases, ACP interacts with AcpS predominantly through helix 2 and is electrostatically driven for AcpS and hydrophobically driven for the Sfp-like PPTases. In the former case, specific interactions between aspartate and glutamate residues on helix 2 of ACP and arginine residues on helix 1 of AcpS are considered important for the formation of the protein complex.[8,40] These residues are highly conserved in a range of ACPs and AcpSs, and they show a similar arrangement around helix α1. When they are superimposed on each other, the position of helix α1 and ML1 is conserved in all of the structures, which all have either CoA (*B. subtilis*, *V. cholerae*, and *S. coelicolor*) or 3′,5′-ADP bound (*B. anthracis* and *St. pneumoniae*), and is distinct from the position of this helix in the *S. coelicolor* apo structure. The conservation of the fold in this critical region between *B. subtilis* AcpS and *Sc* AcpS gave support for the construction of a model for the *S. coelicolor* ACP−AcpS complex as described in Experimental Procedures (Figure 7A). The positive−negative charge recognition is preserved when an AcpS−ACP complex is modeled for *S. coelicolor* by superimposing the ACP (apo

dx.doi.org/10.1021/bi2003668 |*Biochemistry* 2011, 50, 5704–5717

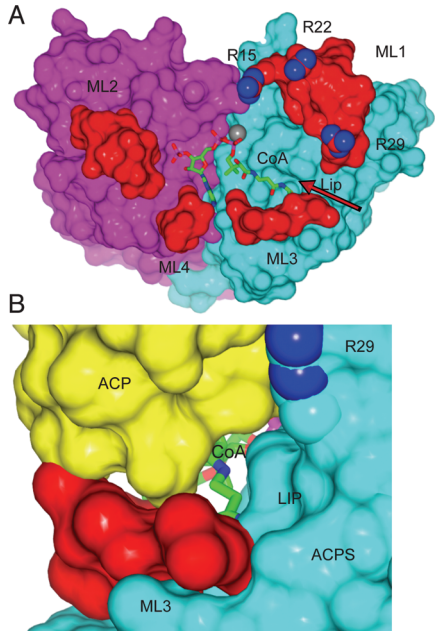

Figure 8. (A) ACP binding site on subunits A and B viewed from above, with *Sc* AcpS in surface representation and CoA shown in bond representation. The nitrogen atoms from the conserved arginines around mobile helix 1 of *Sc* AcpS are colored blue. Regions that are mobile in the ligand-free structure and change between the ligand-free and ligand-bound structures are colored red. (B) Model described in panel A viewed in the direction of the arrow shown in panel A, with ACP also included in space-filling representation in yellow.

closest to the geometric average NMR structure) on *B. subtilis* ACP and the ligand-bound *Sc* AcpS on *B. subtilis* AcpS. ArgB15 can interact with Asp41 (ArgB14 and Asp35 in *B. subtilis*); ArgB22 is close to Glu47 (Arg21 and Glu41 in *B. subtilis*), and ArgB29 can interact with Glu53 (Arg28 with Glu47 in *B. subtilis*) (Figure 7B). *Sc* AcpS is able to phosphopantetheinylate *E. coli* FAS ACP, which has an overall fold similar to that of act ACP.[22,41] Superposition of this ACP provides a comparable picture, with the residues that potentially interact all being conserved and lying in suitable locations.

The activity measurements suggest that Asp41 is the most important residue for the AcpS−ACP interaction, losing 100% of its activity on mutation to an alanine and undergoing a 7-fold reduction in activity upon mutation to a glutamate. Similarly, the reciprocal mutation, R15A, reduced the activity of AcpS to approximately 15% of that of the wild type despite having only a weak effect on CoA binding and the K_d for ACP. Our model suggests that this interaction is important for locking ACP and specifically Ser42 into the correct position for phosphopantetheinylation to occur. Asp41 is in fact located in a region that can swing down to form a salt bridge with ArgB15, bringing Ser42 near the active site. Substitution of the aspartate with a glutamate might affect the precise positioning of Ser42 and could account for the 7-fold reduction in activity. Alternatively, the geometry could be appropriate for Asp41 to act as the base, directly abstracting a proton from Ser42 in preparation for nucleophilic attack on the β-phosphate of CoA. In this model, ArgB15 might complete a catalytic triad. The analogous aspartate, D35, has been mutated to an asparagine in *E. coli* ACP, where it was also observed to abolish activity with *E. coli* AcpS.[42,43] However, several studies have revealed that the more promiscuous Sfp-type PPTases can tolerate an asparagine or serine at this position on the ACP,[43 44] suggesting it is not essential for catalytic activity, at least within the group II enzymes.

Glu53, situated farther from Ser42 at the C-terminus of helix 2, may play a smaller role in the precise positioning of ACP as there is only a 25% loss of activity for the E53A mutant. The reduction in the activity of the D37A mutant is more difficult to rationalize because Asp37 from ACP shows no direct interaction with *Sc* AcpS in our model or analogous cocrystal structures.[8] Instead, the side chain hydrogen bonds with the amide of the residue three positions before it in the primary sequence (i.e., Arg34 in act ACP). This interaction stabilizes a partial turn of α-helix that helps to assemble a core of hydrophobic residues. This conserved acidic residue may therefore be important for preserving an active structure of ACP and correct presentation of Ser42, rather than a direct role in the interaction between ACP and AcpS. We have previously shown that mutation of both D62 and L43 (Table 1) can also have profound effects on activity despite having only modest influences on binding affinity. Because neither of these residues has a catalytic role in the transfer mechanism, this again points to the highly sensitive nature of this interaction to certain key amino acids and hence the orientation of the complexed ACP.

Figure 8A shows a space-filling diagram of subunits A and B, and the positions of the arginines that interact with helix 2 of ACP are highlighted with their nitrogen atoms colored blue. The four areas that change conformation on CoA binding are highlighted in red, and the three arginines are clustered into the top flexible region, ML1, surrounding the active site of *Sc* AcpS. These CoA-driven conformational changes would affect the interaction with the ACP, and therefore, the binding of CoA may act as a structural trigger for the binding of ACP. Inspection of both the *B. subtilis* structures and the *Sc* AcpS−ACP model also suggests that in addition to satisfying this charge alignment, further conformational change needs to take place in the ACP itself to allow Ser42 access to the CoA for phosphoryl transfer to take place.

Promiscuity of *Sc* AcpS for Alternative ACP Partners. The activity of *Sc* AcpS with different ACP partners has been reported previously.[22] *Sc* AcpS was able to recognize *E. coli* FAS ACP, *Streptomyces rimosus* oxytetracycline ACP, the type I FAS ACP from rat, and the fungal type I ACP from the norsellinic acid synthase from *Aspergillus parasiticus*. Although quantitative rates were not measured, the AcpS was able to modify each ACP to 100% holo over a 90 min assay. AcpS must provide a binding site that is sufficiently plastic to allow ACPs with slightly different surface characteristics to bind with the key conserved arginine groups of AcpS. ML3 possesses the flexibility necessary for this initial interaction. In contrast to other structures determined, CoA binding drives a conformational change in ML3 that makes the ACP binding pocket wide and shallow (Figure 8B). Inspection of the alignment of AcpS sequences reveals considerable variability in this region. The sequence of the *S. coelicolor* ML3 region is both shorter and also contains predominantly residues with small side chains, which impart increased flexibility (sequence GAPAG vs GTGIGRQ in *B. subtilis*). Our model also suggests that once AcpS has accommodated CoA no further structural adjustments are necessary for ACP binding. This is in contrast to *B. subtilis*, for which superposition of the holo structure on the ACP−AcpS structure indicates that the 4′-PP portion of CoA has to move to accommodate ACP association. This region of the structure corresponds to the domain-swapped

area that Reuter and co-workers proposed to be responsible for determining the peptidyl carrier protein specificity in the *B. subtilis* Sfp (Figure 5D).[11]

Promiscuity of *Sc* AcpS for Acyl CoAs. *Sc* AcpS can transfer several acyl-phosphopantetheine chains from acyl-CoA to the apo-ACP.[22] In *Sc* AcpS, the 4′-PP chain binds to a pocket that accommodates the chain neatly, and the acetyl-CoA structure demonstrates that it can expand very little to accommodate the extra volume of the modified CoAs known to be transferred (e.g., methylmalonyl- and benzoyl-CoAs). A space-filling representation of the model does, however, illustrate a possible route for the extensions to CoA over the surface of AcpS (Figure 8A) that is not obstructed by the binding of ACP (Figure 8B). The two residues, LeuB70 and ThrB72, that lie on the lip of ML3 do not obstruct this exit route, whereas large charged or polar residues (Arg, Tyr, and Gln) are found in these positions in a range of other AcpSs. Because the CoA binding site is essentially fixed or preformed, a more compact ML3 may be the key to accommodating CoAs with large acyl substituents.

CONCLUSION

Although there have been a number of published studies of the group I AcpSs and a number of deposited structures, a lack of consistency in the bound metal ions and the use of a variety of CoA analogues have meant that there is no reliable representation of a type I phosphopantetheine transferase. The structure of the ligand-bound form of *S. coelicolor* AcpS presented here contains a single magnesium ion and one molecule of CoA per active site and provides the most biologically relevant representation of the enzyme reported to date. This study shows that the *Sc* AcpS forms a homotrimer with an active site formed at the interface of adjacent subunits. The presence of Mg^{2+} at the active site suggests an overall mechanism consistent with the group II PPTases. Critically, GluB57 is available to deprotonate the serine of ACP in preparation for nucleophilic attack at the β-phosphate of CoA, whereas the analogous residue is trapped in the coordination of Ca^{2+} in a previous group I model. The high-resolution structures of both the ligand-free and ligand-bound forms show that the active sites contain a number of mobile loop regions that accommodate binding of the CoA. In the CoA-bound form, the mobile loops reorient to form a pocket that can bind ACP in preparation for phosphopantetheine transfer. This preformed pocket means that the binding of the CoA is not dependent on the interaction with any particular ACP, which was suggested for the *B. subtilis* AcpS. The compact mobile loop, ML3, provides an exit channel that can facilitate the binding of extended acyl-CoAs, allowing us to explain the observed promiscuity of acyl-CoA transfer. ML3 therefore appears to play a role similar to that of the equivalent mobile loop observed in the dimeric human type II phosphopantetheine transferase. Therefore, this study shows that there is a broadly similar active site and binding site architecture between the group I and II PPTases.

ASSOCIATED CONTENT

Supporting Information. Omit $F_o - F_c$ density (colored green) contoured at 3σ, in a sphere 6 Å around the Mg^{2+} (omit map calculated after 10 cycles of refinement with a protein-only model) and isothermal titration calorimetry data showing the presence of a strong binding site for (A) binding of CoA, (B) binding of acetyl-CoA, (C) binding of CoA to the H110A mutant, and (D) binding of CoA to the D111A mutant. This material is available free of charge via the Internet at http://pubs.acs.org.

AUTHOR INFORMATION

Corresponding Author

*A.T.H.: phone, +44 (0)117 951 4253; fax, +44 (0)117 925 1295; e-mail, andrea.t.mulholland@gmail.com. M.P.C.: phone, +44 (0)117 3317163; fax, +44 (0)117 925 1295; e-mail, matt.crump@bristol.ac.uk. J.C.: phone, +44 (0)117 9288445; fax, +44 (0)117 925 1295; e-mail, john.crosby@bristol.ac.uk.

Author Contributions

P.D. and C.J.A. contributed equally to this work.

Funding Sources

This work was supported by the Biotechnology and Biological Sciences Research Council (BB/F014570/1). We also thank the European Union for a studentship grant to P.D. under the Marie Curie Early Training Award scheme ('BRISENZ').

ABBREVIATIONS

act, actinorhodin; ACP, acyl carrier protein; CoA, coenzyme A; rmsd, root-mean-square deviation; FAS, fatty acid synthase; ligand-bound AcpS, AcpS with Mg^{2+} and CoA bound; 4′-PP, phosphopantetheine; PPTase, phosphopantetheinyl transferase; PKS, polyketide synthase; *Sc* AcpS, *S. coelicolor* phosphopantetheinyl transferase.

REFERENCES

(1) Lambalot, R. H., Gehring, A. M., Flugel, R. S., Zuber, P., LaCelle, M., Marahiel, M. A., Reid, R., Khosla, C., and Walsh, C. T. (1996) A new enzyme superfamily: The phosphopantetheinyl transferases. *Chem. Biol. 3*, 923–936.

(2) Elovson, J., and Vagelos, P. R. (1968) Acyl carrier protein. X. Acyl carrier protein synthetase. *J. Biol. Chem. 243*, 3603–3611.

(3) Gilbert, A. M., Kirisits, M., Toy, P., Nunn, D. S., Failli, A., Dushin, E. G., Novikova, E., Petersen, P. J., Joseph-McCarthy, D., McFadyen, L., and Fritze, C. C. (2004) Anthranilate 4H-oxazol-5-ones: Novel small molecule antibacterial acyl carrier protein synthase (AcpS) inhibitors. *Bioorg. Med. Chem. Lett. 14*, 37–41.

(4) Joseph-McCarthy, D., Parris, K., Huang, A., Failli, A., Quagliato, D., Dushin, E. G., Novikova, E., Severina, E., Tuckman, M., Petersen, P. J., Dean, C., Fritz, C. C., Meshulam, T., DeCenzo, M., Dick, L., McFadyen, L. J., Somers, W. S., Lovering, F., and Gilbert, A. M. (2005) Use of structure-based drug design approaches to obtain novel anthranilic acid acyl carrier protein synthase inhibitors. *J. Med. Chem. 48*, 7960–7969.

(5) Arthur, C., Cox, R. J., Crosby, J., Rahman, M. M., Simpson, T. J., Soulas, F., Spogli, R., Szafranska, A. E., Westcott, J., and Winfield, C. J. (2002) Synthesis and characterisation of acyl carrier protein bound polyketide analogues. *ChemBioChem 3*, 253–257.

(6) Zhou, Z., Koglin, A., Wang, Y., McMahon, A. P., and Walsh, C. T. (2008) An eight residue fragment of an acyl carrier protein suffices for post-translational introduction of fluorescent pantetheinyl arms in protein modification in vitro and in vivo. *J. Am. Chem. Soc. 130*, 9925–9930.

(7) Flugel, R. S., Hwangbo, Y., Lambalot, R. H., Cronan, J. E., Jr., and Walsh, C. T. (2000) Holo-(acyl carrier protein) synthase and phosphopantetheinyl transfer in *Escherichia coli*. *J. Biol. Chem. 275*, 959–968.

(8) Parris, K. D., Lin, L., Tam, A., Mathew, R., Hixon, J., Stahl, M., Fritz, C. C., Seehra, J., and Somers, W. S. (2000) Crystal structures of substrate binding to *Bacillus subtilis* holo-(acyl carrier protein) synthase reveal a novel trimeric arrangement of molecules resulting in three active sites. *Struct. Folding Des. 8*, 883–895.

(9) Chirgadze, N. Y., Briggs, S. L., McAllister, K. A., Fischl, A. S., and Zhao, G. (2000) Crystal structure of *Streptococcus pneumoniae* acyl

carrier protein synthase: An essential enzyme in bacterial fatty acid biosynthesis. *EMBO J. 19*, 5281–5287.

(10) Quadri, L. E., Weinreb, P. H., Lei, M., Nakano, M. M., Zuber, P., and Walsh, C. T. (1998) Characterization of Sfp, a *Bacillus subtilis* phosphopantetheinyl transferase for peptidyl carrier protein domains in peptide synthetases. *Biochemistry 37*, 1585–1595.

(11) Reuter, K., Mofid, M. R., Marahiel, M. A., and Ficner, R. (1999) Crystal structure of the surfactin synthetase-activating enzyme sfp: A prototype of the 4′-phosphopantetheinyl transferase superfamily. *EMBO J. 18*, 6823–6831.

(12) Bunkoczi, G., Pasta, S., Joshi, A., Wu, X., Kavanagh, K. L., Smith, S., and Oppermann, U. (2007) Mechanism and substrate recognition of human holo ACP synthase. *Chem. Biol. 14*, 1243–1253.

(13) Murugan, E., and Liang, Z. X. (2008) Evidence for a novel phosphopantetheinyl transferase domain in the polyketide synthase for enediyne biosynthesis. *FEBS Lett. 582*, 1097–1103.

(14) Worsham, L. A. S., Earls, L., Jolly, C., Langston, K. G., Trent, M. S., and Ernst-Fonberg, M. L. (2003) Amino acid residues of *Escherichia coli* acyl carrier protein involved in heterologous protein interactions. *Biochemistry 42*, 167–176.

(15) Zhang, Y. M., Rao, M. S., Heath, R. J., Price, A. C., Olson, A. J., Rock, C. O., and White, S. W. (2001) Identification and analysis of the acyl carrier protein (ACP) docking site on β-ketoacyl-ACP synthase III. *J. Biol. Chem. 276*, 8231–8238.

(16) Rafi, S., Novichenok, P., Kolappan, S., Zhang, X. J., Stratton, C. F., Rawat, R., Kisker, C., Simmerling, C., and Tonge, P. J. (2006) Structure of acyl carrier protein bound to FabI, the FASII enoyl reductase from *Escherichia coli*. *J. Biol. Chem. 281*, 39285–39293.

(17) Arthur, C. J., Williams, C., Pottage, K., Płoskoń, E., Findlow, S. C., Burston, S. G., Simpson, T. J., Crump, M. P., and Crosby, J. (2009) Structure and malonyl CoA-ACP transacylase binding of *Streptomyces coelicolor* fatty acid synthase acyl carrier protein. *ACS Chem. Biol. 4*, 625–636.

(18) Watve, M. G., Tickoo, R., Jog, M. M., and Bhole, B. D. (2001) How many antibiotics are produced by the genus *Streptomyces*? *Arch. Microbiol. 176*, 386–390.

(19) Malpartida, F., and Hopwood, D. A. (1986) Physical and genetic characterization of the gene cluster for the antibiotic actinorhodin in *Streptomyces coelicolor* A3(2). *Mol. Gen. Genet. 205*, 66–73.

(20) Lu, Y. W., Roman, A. K. S., and Gehring, A. M. (2008) Role of phosphopantetheinyl transferase genes in antibiotic production by *Streptomyces coelicolor*. *J. Bacteriol. 190*, 6903–6908.

(21) Bentley, S. D., Chater, K. F., Cerdeno-Tarraga, A. M., Challis, G. L., Thomson, N. R., James, K. D., Harris, D. E., Quail, M. A., Kieser, H., Harper, D., Bateman, A., Brown, S., Chandra, G., Chen, C. W., Collins, M., Cronin, A., Fraser, A., Goble, A., Hidalgo, J., Hornsby, T., Howarth, S., Huang, C. H., Kieser, T., Larke, L., Murphy, L., Oliver, K., O'Neil, S., Rabbinowitsch, E., Rajandream, M. A., Rutherford, K., Rutter, S., Seeger, K., Saunders, D., Sharp, S., Squares, R., Squares, S., Taylor, K., Warren, T., Wietzorrek, A., Woodward, J., Barrell, B. G., Parkhill, J., and Hopwood, D. A. (2002) Complete genome sequence of the model actinomycete *Streptomyces coelicolor* A3(2). *Nature 417*, 141–147.

(22) Cox, R. J., Crosby, J., Daltrop, O., Glod, F., Jarzabek, M. E., Nicholson, T. P., Reed, M., Simpson, T. J., Smith, L. H., Soulas, F., Szafranska, A. E., and Westcott, J. (2002) *Streptomyces coelicolor* phosphopantetheinyl transferase: A promiscuous activator of polyketide and fatty acid synthase acyl carrier proteins. *J. Chem. Soc., Perkin Trans. 1*, 1644–1649.

(23) Crosby, J., Sherman, D. H., Bibb, M. J., Revill, W. P., Hopwood, D. A., and Simpson, T. J. (1995) Polyketide synthase acyl carrier proteins from *Streptomyces*: Expression in *Escherichia coli*, purification and partial characterisation. *Biochim. Biophys. Acta 1251*, 32–42.

(24) Otwinowski, Z., and Minor, W. (1997) Processing of X-ray diffraction data collected in oscillation mode. *Methods Enzymol. 276*, 307–326.

(25) Collaborative Computational Project Number 4. (1994) The CCP4 suite: Programmes for protein crystallography. *Acta Crystallogr. D50*, 760–763.

(26) McCoy, A. J. (2007) Solving structures of protein complexes by molecular replacement with Phaser. *Acta Crystallogr. D63*, 32–41.

(27) Cohen, S. X., Ben Jelloul, M., Long, F., Vagin, A., Knipscheer, P., Lebbink, J., Sixma, T. K., Lamzin, V. S., Murshudov, G. N., and Perrakis, A. (2008) ARP/wARP and molecular replacement: The next generation. *Acta Crystallogr. D64*, 49–60.

(28) Morris, R. J., Perrakis, A., and Lamzin, V. S. (2003) ARP/wARP and automatic interpretation of protein electron density maps. *Methods Enzymol. 374*, 229–244.

(29) Perrakis, A., Harkiolaki, M., Wilson, K. S., and Lamzin, V. S. (2001) ARP/wARP and molecular replacement. *Acta Crystallogr. D57*, 1445–1450.

(30) Cowtan, K. (1994) dm: An automated procedure for phase improvement by density modification. *Joint CCP4 and ESF-EACBM Newsletter on Protein Crystallography 31*, 34–38.

(31) Emsley, P., and Cowtan, K. (2004) Coot: Model-building tools for molecular graphics. *Acta Crystallogr. D60*, 2126–2132.

(32) Murshudov, G. N., Vagin, A. A., and Dodson, E. J. (1997) Refinement of macromolecular structures by the maximum-likelihood method. *Acta Crystallogr. D53*, 240–255.

(33) Storoni, L. C., McCoy, A. J., and Read, R. J. (2004) Likelihood-enhanced fast rotation functions. *Acta Crystallogr. D60*, 432–438.

(34) McCoy, A. J., Grosse-Kunstleve, R. W., Storoni, L. C., and Read, R. J. (2005) Likelihood-enhanced fast translation functions. *Acta Crystallogr. D61*, 458–464.

(35) Qiu, X. Y., and Janson, C. A. (2004) Structure of apo acyl carrier protein and a proposal to engineer protein crystallization through metal ions. *Acta Crystallogr. D60*, 1545–1554.

(36) Leavitt, S., and Freire, E. (2001) Direct measurement of protein binding energetics by isothermal titration calorimetry. *Curr. Opin. Struct. Biol. 11*, 560–566.

(37) Evans, S. E., Williams, C., Arthur, C. J., Burston, S. G., Simpson, T. J., Crosby, J., and Crump, M. P. (2008) An ACP structural switch. Conformational differences between the apo and holo forms of the actinorhodin polyketide synthase acyl carrier protein. *ChemBioChem 9*, 2424–2432.

(38) Mofid, M. R., Finking, R., Essen, L. O., and Marahiel, M. A. (2004) Structure-based mutational analysis of the 4′- phosphopantetheinyl transferases Sfp from *Bacillus subtilis*: Carrier protein recognition and reaction mechanism. *Biochemistry 43*, 4128–4136.

(39) Cleland, W. W., and Hengge, A. C. (2006) Enzymatic mechanisms of phosphate and sulfate transfer. *Chem. Rev. 106*, 3252–3278.

(40) Hadfield, A. T., Limpkin, C., Teartasin, W., Simpson, T. J., Crosby, J., and Crump, M. P. (2004) The crystal structure of the actIII actinorhodin polyketide reductase: Proposed mechanism for ACP and polyketide binding. *Structure 12*, 1865–1875.

(41) Kim, Y., Kovrigin, E. L., and Eletr, Z. (2006) NMR studies of *Escherichia coli* acyl carrier protein: Dynamic and structural differences of the apo- and holo-forms. *Biochem. Biophys. Res. Commun. 341*, 776–783.

(42) Gong, H., Murphy, A., McMaster, C. R., and Byers, D. M. (2007) Neutralization of acidic residues in helix II stabilizes the folded conformation of acyl carrier protein and variably alters its function with different enzymes. *J. Biol. Chem. 282*, 4494–4503.

(43) De Lay, N. R., and Cronan, J. E. (2007) In vivo functional analyses of the type II acyl carrier proteins of fatty acid biosynthesis. *J. Biol. Chem. 282*, 20319–20328.

(44) Shields, J. A., Rahman, A. S., Arthur, C. J., Crosby, J., Hothersall, J., Simpson, T. J., and Thomas, C. M. (2010) Phosphopantetheinylation and specificity of acyl carrier proteins in the mupirocin biosynthetic cluster. *ChemBioChem 11*, 248–255.